Available online at www.sciencedirect.com
ScienceDirect
Trans. Nonferrous Met. Soc. China 28(2018) 613−628
Transactions of Nonferrous Metals Society of China
www.tnmsc.cn

Effect of tool plunge depth on joint formation and mechanical performance of friction stir forming joints made between AA 5052-H32 and AA 6061-T6 sheet metals

Tinu P. SAJU, R. Ganesh NARAYANAN

Department of Mechanical Engineering, Indian Institute of Technology Guwahati, Assam 781039, India

Received 7 March 2017; accepted 14 July 2017

Abstract: The potential of friction stir forming for joining dissimilar grades of aluminum alloys namely, AA 5052-H32 and AA 6061-T6, was investigated. Study on the effect of tool plunge depth revealed that, lap shear load of 7.16 kN and cross-tensile load of 3.51 kN, recorded at medium tool plunge depth range from 0.5 to 0.7 mm, measured using a universal testing machine, were much larger than those of friction stir welded and friction stir spot welded joints fabricated on the same materials. Joint macrostructure observed with optical microscope revealed that joints were strengthened either by mechanical pin interlocking or by metallurgical bonding. The effect of tool plunge depth on the stir zone formation and the influence of frictional heat flux on the lower sheet were revealed through the microhardness measurement using Vickers hardness tester. Morphological studies revealed that tool plunge depth has a significant influence on the pin formation and the geometric features, generated in these joints. Occurrence of various failure modes such as pin pull-out, pin shear, partial bond delamination, and tear-off, were governed by the formation of critical weak zones at various tool plunge depths.

Key words: friction stir forming; tool plunge depth; aluminum alloy; lap shear test; cross-tension test; failure modes

1 Introduction

Solid state joining using a stir tool such as friction stir welding (FSW) and its variants such as friction stir spot welding (FSSW) and friction stir processing have acquired wide popularity over the past few decades. These processes have emerged as low heat input alternatives to fusion welding techniques. In the early stages of its development, primary focus was on joining softer materials like aluminum, magnesium and copper.

Many experimental studies and constitutive models have been developed on FSW and FSSW of aluminum alloys to accurately predict the joint formation and reveal the effect of significant process parameters. Literature shows that tool plunge depth (TPD) has significant influence on the formation of FSSW. RAO et al [1] reported that the lap shear fracture strength of FSSW joints between AA 6022-T4 wrought aluminum alloy and AM60B cast magnesium alloy increased with increase in TPD at a tool rotational speed of 1000 r/min. It was revealed that increase in TPD had increased the frictional heat flux and the bond width of the joint, which resulted in increase in the joint strength by the interlocking of hard and brittle intermetallic compounds. Increase in the tensile shear fracture load, up to a maximum of 3.07 kN, with increasing TPD was reported from the FSSW of galvanized steel sheets performed by BAEK et al [2]. However, MITLIN et al [3] reported that the excessive tool penetration reduced the tensile shear strength of friction spot welded AA 6111 aluminum sheets, due to hole formation at the stir spot. TPD also has a strong influence on the failure modes. As the TPD increased, the failure mode changed from brittle fracture near the pin hole to ductile fracture away from the weld. TUTAR et al [4] reported that TPD has the highest influence than dwell time and tool rotational speed on the tensile shear failure strength of FSSW samples. Increase in the TPD enhanced stirring of the metals and resulted in wider stir zone, heat affected zone and thermo-mechanically affected zone, thereby increasing the shear strength of FSSW in AA 3003-H12 aluminum alloys. The FSSW of AA 5182-O aluminum alloy sheets performed by BOZZI et al [5] revealed that increasing shoulder plunge depth resulted in initial increase and further decrease in tensile shear strength. Too high shoulder plunge depth resulted

Corresponding author: R. Ganesh NARAYANAN; Tel: +91-361-2582669; E-mail: ganu@iitg.ernet.in
DOI: 10.1016/S1003-6326(18)64694-1

in the excessive localized thinning of the upper sheet. YOON et al [6] reported that probe plunge depth affects the bond width. In addition to the influence on tensile shear failure load, TPD has a remarkable influence on surface appearance and macrostructure of friction stir spot joined AA 5454-O aluminum alloy sheets, while variation in hardness at the joint zone was insignificant. FSSW of AA 5052−AA 6063 aluminum sheet combination performed by PICCINI et al [7] revealed that increase in TPD resulted in increase in the peel strength. In addition, the fracture mechanism changes from interfacial to circumferential with increase in TPD. PATHAK et al [8] also reported an increase in the lap shear strength of FSSW samples in AA 5754 aluminum alloy with increasing TPD. The influence of tool pin profile on the lap shear strength of these FSSW samples under varying TPDs was also studied. The stir tools with cylindrical pin showed better strength than that with tapered cylindrical pin. During the FSSW of AA 5052 aluminum alloy to polyethylene terephthalate, it was reported by YUSOF et al [9] that increase in TPD resulted in tight sticking of polymer to the metal sheet and further resulted in increase in tensile shear strength. ARICI and MERT [10] reported that increase in TPD increased the heat generation and enhanced the plastic deformation in polypropylene sheets with FSSW.

Friction stir forming (FSF) is one of the latest thermo-mechanical spot joining processes for fabricating lap joints in similar and dissimilar sheet metal combinations. The basic principle of this process involves frictional heat generation by stirring and extrusion of the plasticized work material. NISHIHARA [11] conducted initial attempts on friction stir forming (FSF) in 2003. This solid state joining process is eco-friendly and relatively cheap process with less added mass, since the need for external consumables such as rivets, bolts and electrodes are eliminated. Thus, process can be utilized for lightweight applications in automobile industry to achieve better fuel efficiency and reduced CO_2 emission.

The process possesses similarities with FSSW although discrete differences can be observed from the intrinsic features of the FSF joints. Unlike FSSW, stirring in an FSF process plasticizes the upper and lower sheet metals other than the mixing of the stirred metal from the upper and lower sheets. Since the filling of the anvil cavity feature in FSF process requires low volume of plasticized metal, the tool indentation required is negligible as compared to the keyhole left by the pin tool in FSSW process. Moreover, FSF is usually performed with a pinless flat tool.

The following literature describes the recent attempts carried out on FSF process. The cladding of AA 6061-T6 over S45C steel sheet by traversing FSF was conducted by NISHIHARA and ITO [12]. The die temperature measurements showed that maximum temperature up to 740 °C was recorded at 705 r/min and traverse speed of 150 mm/min. BALAKRISHNAN et al [13] fabricated friction stir spot joints with mechanical interlock between aluminum and nylon sheets. Lap shear strength of these joints was higher than that of adhesive bonded joints. FSF joints between zinc coated mild steel sheet and aluminum alloys, namely AISI 5182 and AA 6014, were fabricated by LAZEREVIC et al [14]. Braze welding between the upper and lower sheet was also formed by the diffusion of zinc from the mild steel coating to upper aluminum alloy sheet. A study on the effect of process parameters such as tool plunge depth, tool diameter and anvil cavity depth on FSF joints between dissimilar sheets were reported by LAZAREVIC et al [15]. Tungsten−copper composite was fabricated by AHUJA et al [16] with traversing FSF using pinless stir tool rotating at 1200 r/min and traverse speed of 100 mm/min. OGATA et al [17] applies design of experiments methodology to quantify the operational parameters affecting FSF between dissimilar sheet metals like aluminum to steel. It was reported that tool diameter, plunge depth and anvil cavity geometry have significant effects on FSF joint formation. A decline in the force and torque during anvil cavity filling was also observed.

The exact process analysis and the effect of critical process parameters such as tool plunge depth, tool shoulder diameter on the quality of FSF joint are not yet elaborately studied. Moreover, there is limited literature available on FSF. Therefore, a detailed study for finding the effect of TPD on FSF is worth to be conducted.

AA 5052-H32 and AA 6061-T6 are the commonly used aluminum alloys in automotive and aerospace industries. The present work focuses on studying the effect of tool plunge depth on the mechanical performance of FSF joints between these dissimilar grade aluminum alloys. FSW of AA 6061 aluminum alloys conducted by DAS et al [18] revealed that the heat input during friction stir welding has significant influence on ultimate tensile strength and fatigue behaviours. ILANGOVAN et al [19] reported that FSW of AA 6061−AA 5086 aluminum alloys showed defect free stir zone with improved hardness. They also added that higher grain boundary fraction and formation of brittle intermetallic phases improved the hardness at the weld zone. HEJAZI et al [20] utilized microhardness mapping to predict the microstructure and mechanical properties of AA 6061 FSW sheets through mathematical equations. Two-dimensional contour of grain size and three-dimensional mapping of ultimate tensile strength and yield strength were plotted, which showed good agreement with experimental results. They

also conducted double sided FSW of AA 6061−T913 alloy [21].

FSF joining of dissimilar materials such as aluminum to steel is attempted until now. FSF joining as applied to dissimilar grade alloys of same metal, namely aluminum, is a new attempt. Lap shear test, cross-tension test, peel test and uniaxial tensile test were conducted to evaluate the mechanical performance of the joint at various tool plunge depths. The joint formation has been characterized by optical macrostructures. The hardness measurement across the joints formed and joint morphology have also been presented.

2 Methodology

2.1 Principle

Stirring with a pinless tool generates frictional heat and plasticizes the upper sheet metal. Plasticized metal is forged and extruded through the pre-drilled hole in the lower sheet during the downward tool plunge. The extruded metal fills the anvil cavity and a mechanical pin interlock is produced. In addition, a metallurgical bond is established between the upper and lower sheets. The process sequence is schematically illustrated in Fig. 1. There is a provision for producing single pin and multi pin configurations. The strength of the joint solely depends on process parameters such as tool rotational speed, tool plunge depth, tool profile and anvil cavity design.

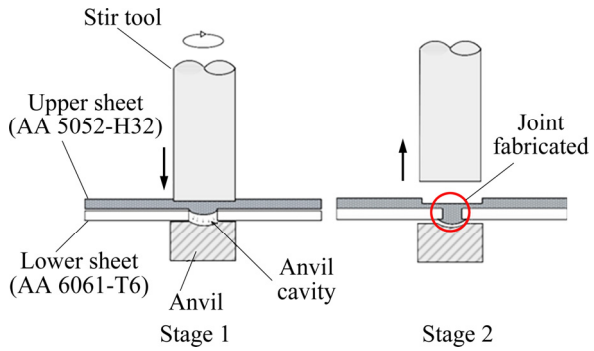

Fig. 1 Schematic diagram of friction stir forming stages

2.2 FSF Experiments

Sample preparation was carried out on a milling machine (Kirloskar Viking KTM 40), for which a customized mild steel fixture capable of holding various metal strips of required dimensions was fabricated. In the experimental setup, the rectangular fixture holds an anvil block on its diagonal center. For pin interlock formation, a cavity with hemispherical shape is machined on the center of the anvil block. The pinless friction stir tool, fixture, anvil and clamps constitute the basic experimental setup, as shown in Fig. 2. The details about anvil and stir tool features are given in Table 1. The anvil cavity size and the stir tool dimensions are selected based on preliminary trials.

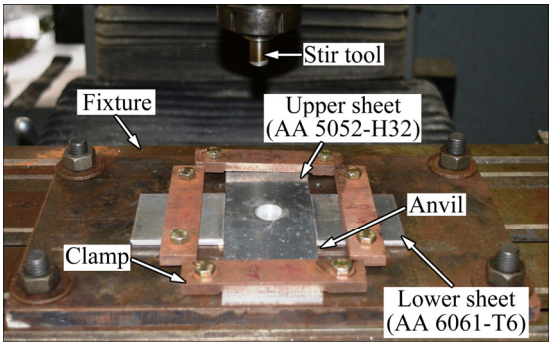

Fig. 2 Experimental setup for FSF process for cross-tensile specimen

AA 5052-H32 and AA 6061-T6 aluminum alloy sheets, each of 2 mm in thickness are used as upper and lower sheets, respectively, since AA 5052-H32 possesses lower tensile yield strength, strength coefficient and hardness than AA 6061-T6. The chemical composition, determined through EDX analysis on Zeiss Sigma 002−B field emission scanning electron microscope and the mechanical properties of these alloys, obtained through standard tensile tests (ASTM−E8), are given in Table 2 and Table 3, respectively.

The sample dimensions of lap shear, cross-tension and peel test are shown in Fig. 3, where the sheet rolling direction is oriented along the length of the samples. Samples were prepared as per AWS D8.9−97 standard. The axis of the FSF joint passes through the stir spot center along a plane perpendicular to the sheet. Pre-drilled hole on the lower sheet was of 3 mm in diameter. The stir tool center, pre-drilled hole center on lower sheet and anvil cavity center are to be aligned along a straight line to enable proper joint formation. The

Table 1 Anvil and stir tool features

Tool				Anvil			
Material	Feature	Shoulder diameter/mm	Shoulder length/mm	Material	Feature	Cavity diameter/mm	Cavity depth/mm
H13 tool steel	Pinless	14	25	Mild steel	Hemispherical cavity on upper surface center	3.5	0.55

Table 2 Chemical composition of sheet metals (mass fraction, %)

Alloy	Si	Fe	Cu	Mn	Mg	Cr	Zn	Ti	Al
AA 5052-H32	≤ 0.2	0.1− 0.3	≤ 0.2	0.1−0.2	2.8−4.2	0.2−0.3	≤ 0.3	−	Bal.
AA 6061-T6	0.6−0.9	0.2−0.4	0.2−0.3	≤ 0.1	1.4−1.8	0.1−0.4	≤ 0.2	≤ 0.15	Bal.

Table 3 Mechanical properties of sheet metals (along 0° rolling direction)

Alloy	Tensile yield strength/MPa	Ultimate tensile strength/MPa	Total elongation/%	Micro-hardness (HV)	Strain hardening exponent, *n*	Strength coefficient, *K*/MPa	Plastic strain ratio, *R*
AA 6061-T6 (lower sheet)	225±13	308±5	21.4±7	99.8±6	0.15±0.003	489±8	0.71
AA 5052-H32 (upper sheet)	155±2	212±2	14.8±1	77.4±9	0.16±0.002	355±6	0.59

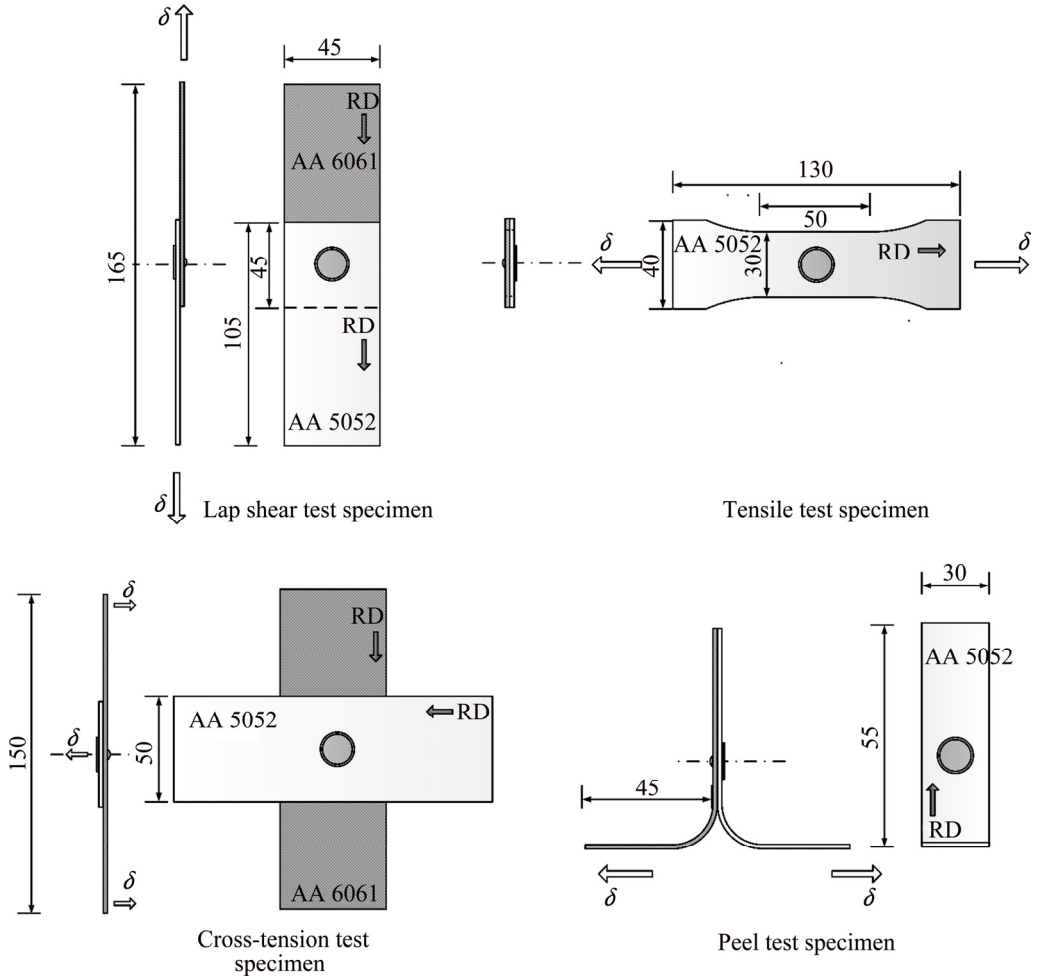

Fig. 3 Dimensions of samples for mechanical performance test (unit: mm)

effect of tool plunge depth on the effectiveness of the FSF joint formation was studied by varying the tool plunge depth at various levels with lower levels at 0.2 and 0.3 mm, medium levels at 0.5 and 0.7 mm and higher levels at 0.9 and 1.1 mm. The attempts to fabricate FSF samples at 0.1 mm failed, due to the absence of any mechanical pin formation. Therefore, the lowest TPD was set to be 0.2 mm. It is the lowest TPD at which the chance of formation of a sound FSF joint is possible for the combination of 2 mm-thick aluminum sheets. All other parameters namely plunge rate, tool rotational speed, direction of tool rotation were kept constant at 0.002 mm/s, 500 r/min and clockwise direction, respectively. Tool plunge rate was chosen based on experimental trials to ensure that the deformation in the lower sheet is minimum. Tool rotational speed and direction of tool rotation were selected as per results obtained from previous work [22].

Two samples were fabricated per TPD for all the tests and the average output value was considered.

2.3 Mechanical performance tests

Lap shear test and cross-tension test are commonly used for evaluating the strength of a lap joint, where the tensile load is applied perpendicular and parallel to the axis of the FSF joint, respectively. It was ensured that the lap shear, cross-tension and peel test samples failed at the joint location only. The formability of the FSF samples under uniaxial tensile loading was determined by conducting tensile test.

All the mechanical performance tests were carried out on a 100 kN Instron-dynamic universal testing machine (Model: 8801J4051), where the extension rate was kept at standard value of 1 mm/min. In all the mechanical performance tests, the load-progression data were recorded and the modes of failure were observed.

2.4 Macrostructure, hardness measurement and joint morphology analysis

Sample preparation for macrostructure analysis was done as per ASTM E407−07 standard. The stir spot cross-sections were subjected to rough finishing with emery paper up to 2000 grade followed by fine finishing with velvet cloth. The polished samples were etched for 20 s with Kellers reagent (190 mL distilled water, 5 mL HNO_3, 3 mL HCl and 2 mL HF). The macrostructure images were taken using optical microscope (Zeiss Axiocam MR3). The metal flow, zone formation and defects were revealed.

Vickers hardness measurements were taken at 0.5 N load for 10 s using Buehler MMT3−B micro Vickers hardness tester. Measuring conditions were selected as per ASTM E92−16 standard. Indentations were performed in two arrays with 2 mm spacing in between the indentations. Upper array covers the upper sheet (locations 1−15 in Fig. 4(a) for lower level TPDs and locations A−O in Fig. 4(b) for medium and higher level TPDs). Lower array covers the lower sheet (locations 16−24 in Fig. 4(a) for lower TPDs and locations P−X in Fig. 4(b) for medium and higher TPDs).

Joint morphology analysis involves the quantification of certain external macroscopic joint features, whose formation is profoundly influenced by the TPD, using a USB digital microscope (Dinolite-DinoCapture 2). These morphological features include macro defects such as lower sheet flash (includes lower sheet flash width and lower sheet flash height), upward bulging of upper sheet and structural features such as mechanical pin extrudate (includes pin width and pin height) and stir spot thickness. The joint features are represented over typical FSF joint cross-sections, as shown in Fig. 5.

3 Results and discussion

This section deals with the effect of TPD on the joint strength, extension at failure and failure modes of FSF samples obtained through four different mechanical performance tests, macrostructure analysis, hardness measurement and morphological study of joint features.

3.1 Mechanical performance tests

Figures 6 and 7 show the effect of TPD on the fracture load (joint strength) and extension at failure

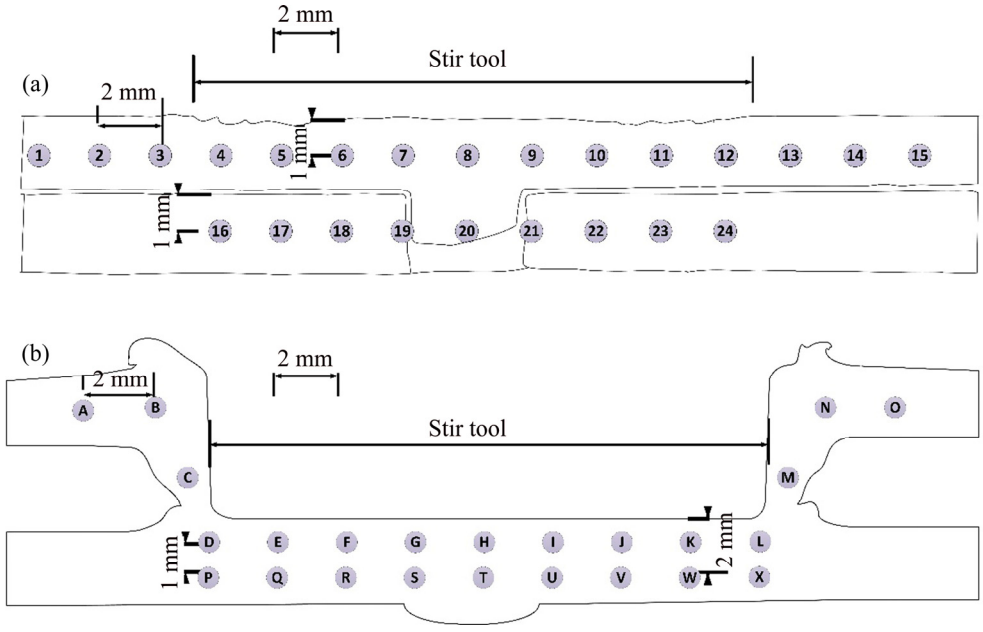

Fig. 4 Hardness measurement locations along joint cross-sections: (a) Lower TPD (0.2, 0.3 mm) samples; (b) Medium (0.5, 0.7 mm) and higher (0.9, 1.1 mm) TPD samples

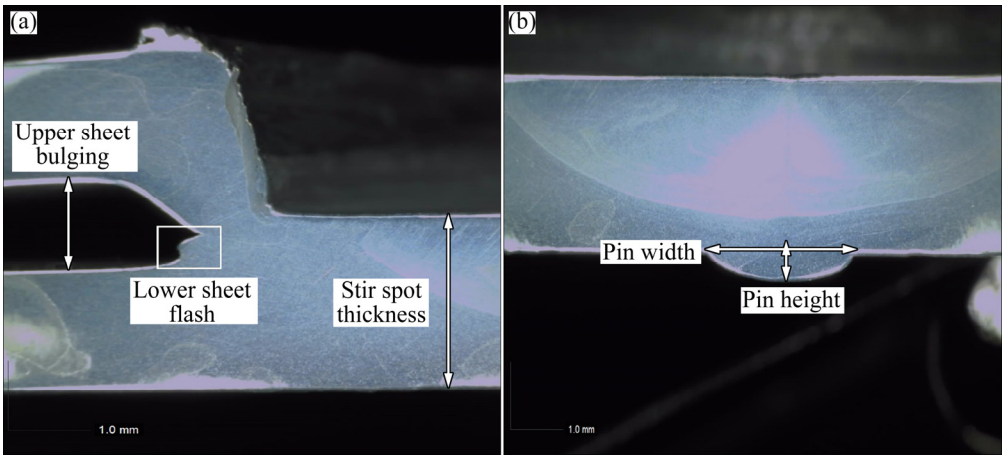

Fig. 5 Morphological features of joint cross-section

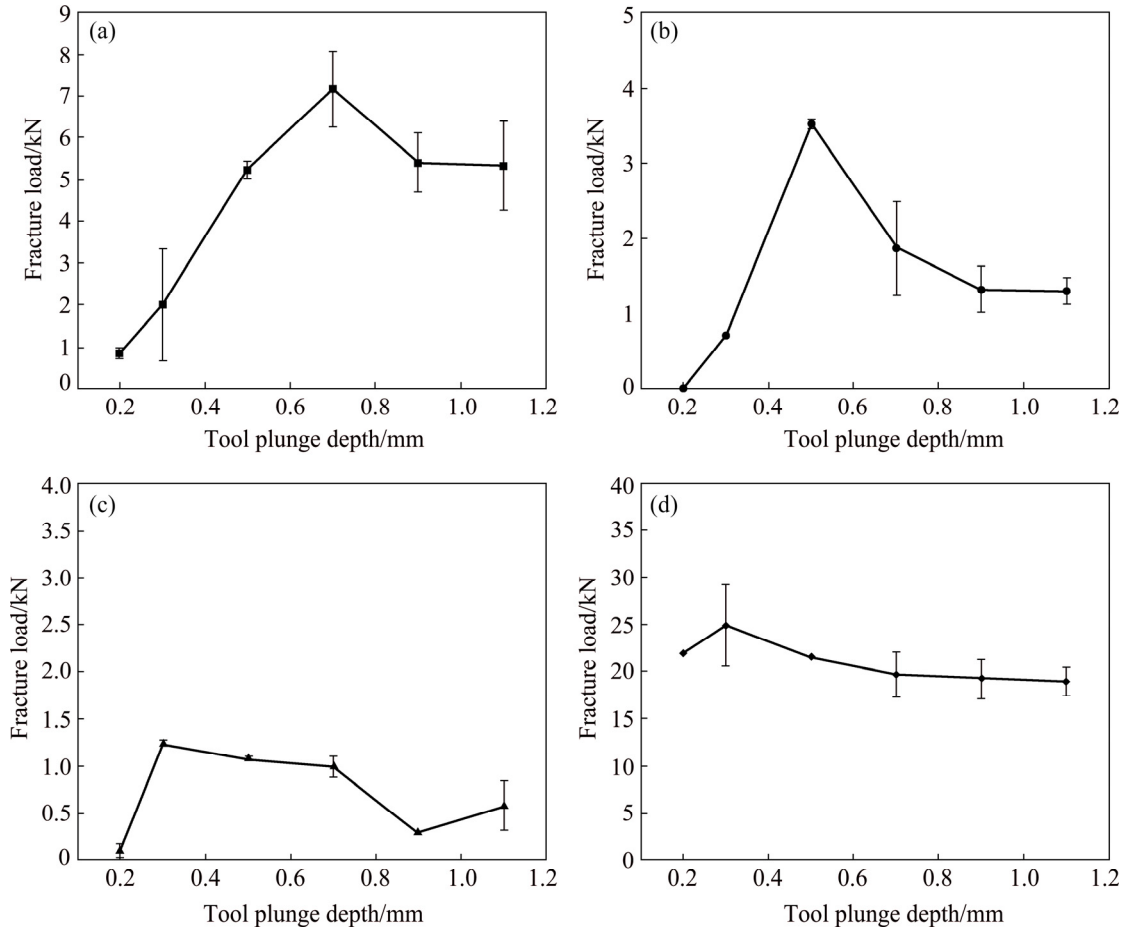

Fig. 6 Comparison of fracture loads at various TPDs during mechanical tests: (a) Lop shear test data; (b) Cross-tension test data; (c) Peel test data; (d) Tensile test data

obtained from mechanical performance tests. It is observed from Fig. 6 that there is an optimum TPD range, between 0.5 and 0.7 mm, within which the joint strength is maximum. Such maximum joint strength changes slightly with the testing methods. For instance, in lap shear test, the fracture load is maximum at 0.7 mm TPD and it decreases at any TPD, higher and lower than the optimum one. There is about 700% increase in fracture load, when the TPD is increased from 0.2 mm (0.86 kN) to 0.7 mm (7.16 kN). Similarly, in the case of cross-tension test, the optimum joint strength occurs at 0.5 mm TPD. There is about 350% increase in the cross-tension load, when the TPD is increased from 0.2 to 0.5 mm. The change in fracture load (or joint strength)

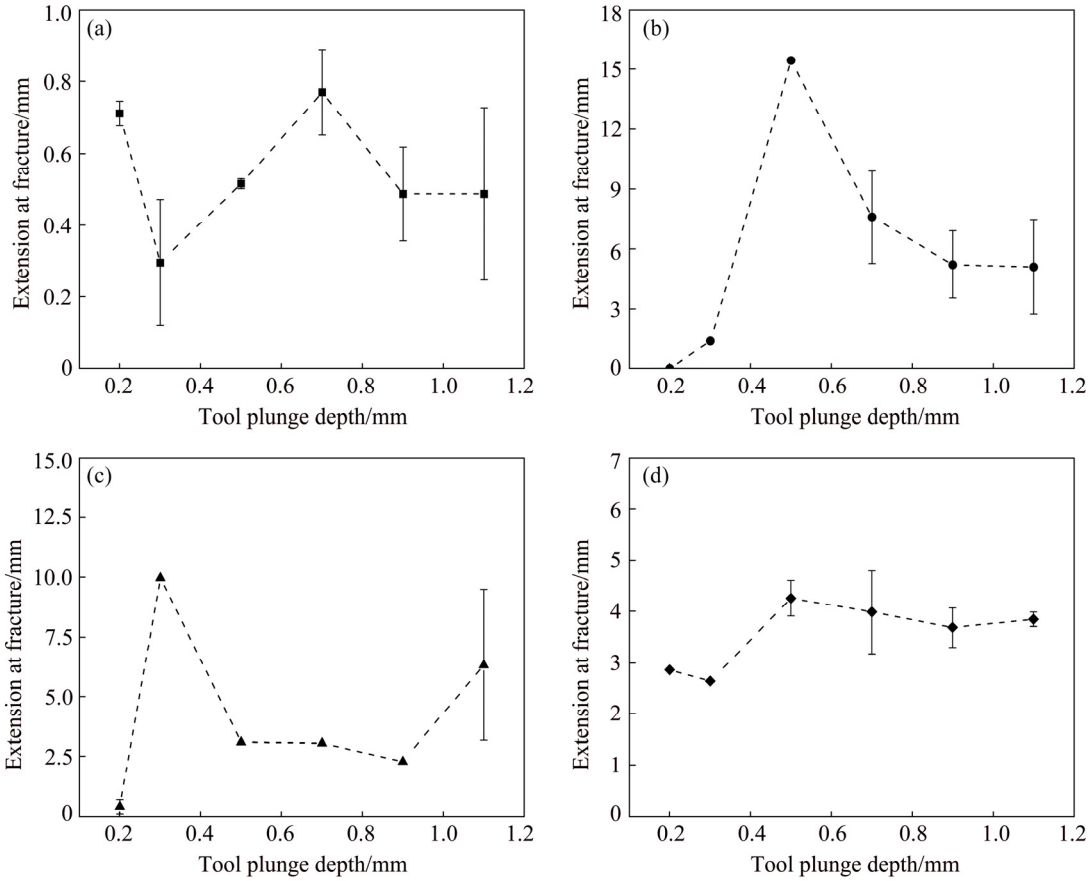

Fig. 7 Comparison of extension at fracture loads for various TPDs during mechanical tests: (a) Lop shear test data; (b) Cross-tension test data; (c) Peel test data; (d) Tensile test data

is not significant in peel test, though maximum fracture load occurs at 0.3 mm TPD. The variation in peel load is within 1 kN, when the TPD is varied during the peel test. Sound joint strength is attained at higher TPD range (0.9−1.1 mm) during lap shear test and cross-tension test. But, peel test samples show poor strength at this TPD range, which is not acceptable. At medium TPD range from 0.5 to 0.7 mm, the joint strength is optimum during lap shear test and cross-tension test, while peel test samples show fairly better joint strength. Variation in joint strength within the medium TPD range is also observed during these three tests, which is not significant, since the values fall in acceptable range of joint strength. Unlike these three tests, the tensile tests denote the forming performance of samples with an FSF joint. In this case, the joint strength decreases from 0.3 to 1.1 mm TPD. A decrease of 24% within the range is seen, showing the importance of TPD on the forming performance. Such a decrease is directly related to the geometrical heterogeneity developed within the stir spot.

It is seen from Fig. 7 that extension at failure changes significantly with change in TPD and the optimum value also changes, though within a range, with respect to the tests performed. For example, optimum TPDs of 0.7, 0.5 and 0.3 mm are obtained in the case of lap shear tests, cross-tension tests and peel tests, respectively. There is a considerable decrease in extension at failure other than at optimum TPDs. To be specific, about 62% and 77% decrease in extension at fracture is seen in cross-tension tests and peel tests, when the TPD is increased from optimum value. In the case of tensile tests, though the variation in extension at failure is insignificant, an optimum TPD of 0.5 mm can be fixed.

It can be noted that the TPD range at which the fracture strength and extension at failure are maximum, for different mechanical tests, is almost same. Also, the fracture load is observed to be the highest during lap shear test and the lowest during peel test. Cross-tension test data falls in between in most of the cases. From the analysis, it can be concluded that the optimum TPD to obtain a strong joint with acceptable extension for AA 5052-H32−AA 6061-T6 combination is in the moderate range of 0.5−0.7 mm. The main reason for the effect of TPD on the joint strength and extension at failure is found to be the pin interlock formation and metallurgical bonding and the same has been explained in Section 3.2.

Joining of AA 5052-H32 to AA 6061-T6 with FSW and FSSW was already attempted. Table 4 gives a comparison of joint strength of these joints with FSF joints of the present work. It is observed that FSF joints possess superior joint strength over FSW and FSSW.

Table 4 Comparison of joint strength of FSF with other joining technologies

Joining technique	Joint form	Test type	Average load/kN	Source
Friction stir welding	Butt joint	Tensile test	5.75	[23]
Friction stir welding	Butt joint	Tensile test	4.85	[24]
Friction stir welding	Butt joint	Tensile test	5.93*	[25]
Friction stir spot welding	Lap joint	Lap shear test	4.85	[26]
Friction stir forming	Lap joint	Lap shear test	7.16	Present work

*Calculated from average tensile strength in MPa

3.2 Joint formation through macrostructure analysis

The FSF joint formation under increasing TPD is explained with the macrostructure analysis. FSF samples fabricated at each of the low, medium and high TPDs are selected for macrostructure analysis. The various zones that can be commonly identified in an FSF joint cross section are stir zone (SZ), thermo-mechanically affected zone (TMAZ) and plastically deformed metal flow zone (PDZ). The complete macrostructure of the FSF joint cross-section, with schematic representation of various zones and metal flow directions are shown in Fig. 8 and Fig. 9, respectively.

3.2.1 Lower TPDs: 0.2 and 0.3 mm

The joint macrostructure and schematic of metal flow in lower TPDs are shown in Figs. 8(a), (b) and Figs. 9(a), (b), respectively. At 0.2 mm TPD, the pin formation has just started. The plastically-deformed upper sheet has partially filled the pre-drilled hole in the lower sheet, and no mechanical interlocking has been established. The anvil cavity is not filled with the extruded upper sheet metal, as it is generally required in FSF. At the end, there is no metallurgical bonding seen at the interface. Since the TPD is insufficient, the SZ is small and confined to the top of the upper sheet. The flash formation is absent. The partial extrusion of upper sheet in the form of pin has generated a prominent PDZ.

With further increase in TPD to 0.3 mm, the extruded pin has almost reached the bottom of the anvil cavity and filled the pre-drilled hole fully. The SZ size has increased to such an extent that the hole has deformed partially to initiate a mechanical interlocking around the neck of the pin. The upper sheet flash has been generated without TMAZ formation.

Since there is no metallurgical bonding between the two sheets, the joint strength and extension at failure is lower under these TPDs. The mechanical interlocking has solely contributed to such a lower joint strength and extension at failure.

3.2.2 Moderate TPDs: 0.5 and 0.7 mm

Figures 8(c), (d) and Figs. 9(c), (d) show the joint macrostructure and metal flow directions for moderate TPDs, respectively. With further increase in TPD to 0.5 mm, the metallurgical bonding has been initiated between the two sheets. The anvil cavity is also filled by the pin extruded. But the TPD is severe enough to completely deform the hole and it closes the pin path. Hence, the connection between the pin and the upper sheet is lost in between. The lower sheet has also deformed and filled the anvil cavity, which is generally not expected in FSF. On the other hand, the SZ and TMAZ size have increased. The upward distortion of lower sheet and upward bulging of upper sheet are seen prominently. The upper sheet flash has increased further. At 0.7 mm TPD, there is nothing new occurring in the joint formation. The disconnected pin has deformed further. The SZ, TMAZ, upper sheet flash, upward bulging of upper sheet and upward distortion of the lower sheet have increased further in their sizes.

It can be observed that direction of tool rotation has an influence on the deformation of the PDZ. The disconnected PDZ has been deviated to the left hand side of the cross section, as seen in Figs. 8(c) and (d), because of the clockwise direction of rotation of the stir tool along with the downward tool plunge. Under these TPDs, reasonably good joints are fabricated with improved joint strength and extensibility. Such an improvement is mainly contributed by metallurgical bonding.

3.2.3 Higher TPDs: 0.9 and 1.1 mm

The joint macrostructure and schematic of metal flow in higher TPDs are shown in Figs. 8(e), (f) and Figs. 9(e), (f), respectively. At higher TPDs of 0.9 and 1.1 mm, the SZ size has increased further, resulting in the merging of upper sheet to the extruded pin. The metallurgical bonding between the upper and lower sheets exists in these TPDs as well. Like in the moderate TPDs, the TMAZ, upward bulging of upper sheet, upper sheet flash have increased in their dimensions. The lower sheet flash formation has also been observed in these TPDs. In spite of having a good metallurgical bonding and mechanical interlocking at higher TPDs, the joint strength is inferior than that in moderate TPDs. This is because of the upward distortion of lower sheet creating a separation between the SZ at center and the side walls of the stir spot circumference, thereby creating a material discontinuity ‘CR3’ at both the ends of SZ (Fig. 9(f)).

Just to summarize, the SZ formation, metallurgical bonding and pin interlocking govern the effect of TPD and joint performance during mechanical testing. The joint performs better at moderate TPDs (0.5 and 0.7 mm) because of good metallurgical bonding. At lower TPDs (0.2 and 0.3 mm), the metallurgical bonding and

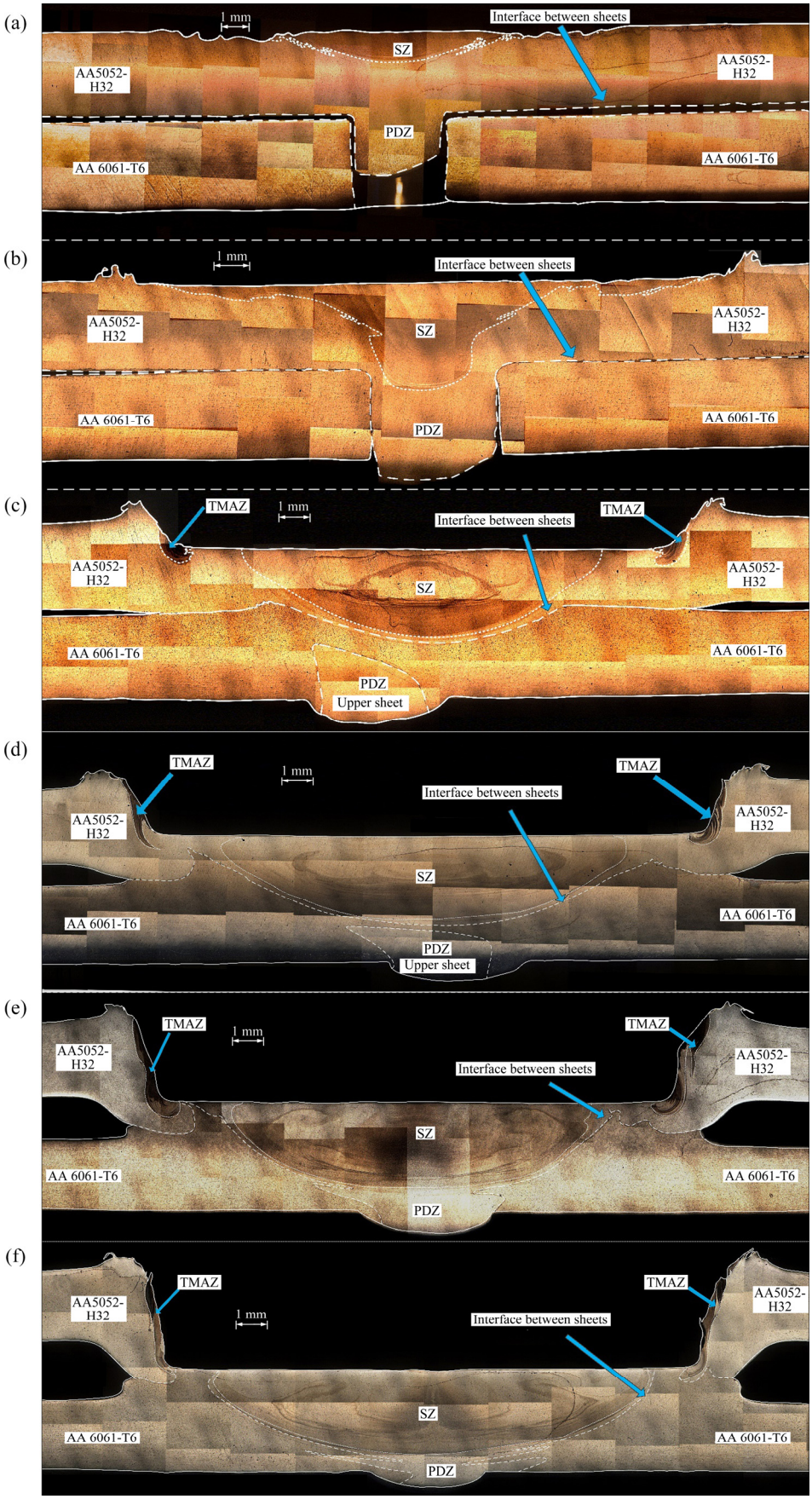

Fig. 8 Joint macrostructures of FSF samples fabricated at different TPDs: (a) 0.2 mm; (b) 0.3 mm; (c) 0.5 mm; (d) 0.7 mm; (e) 0.9 mm; (f) 1.1 mm

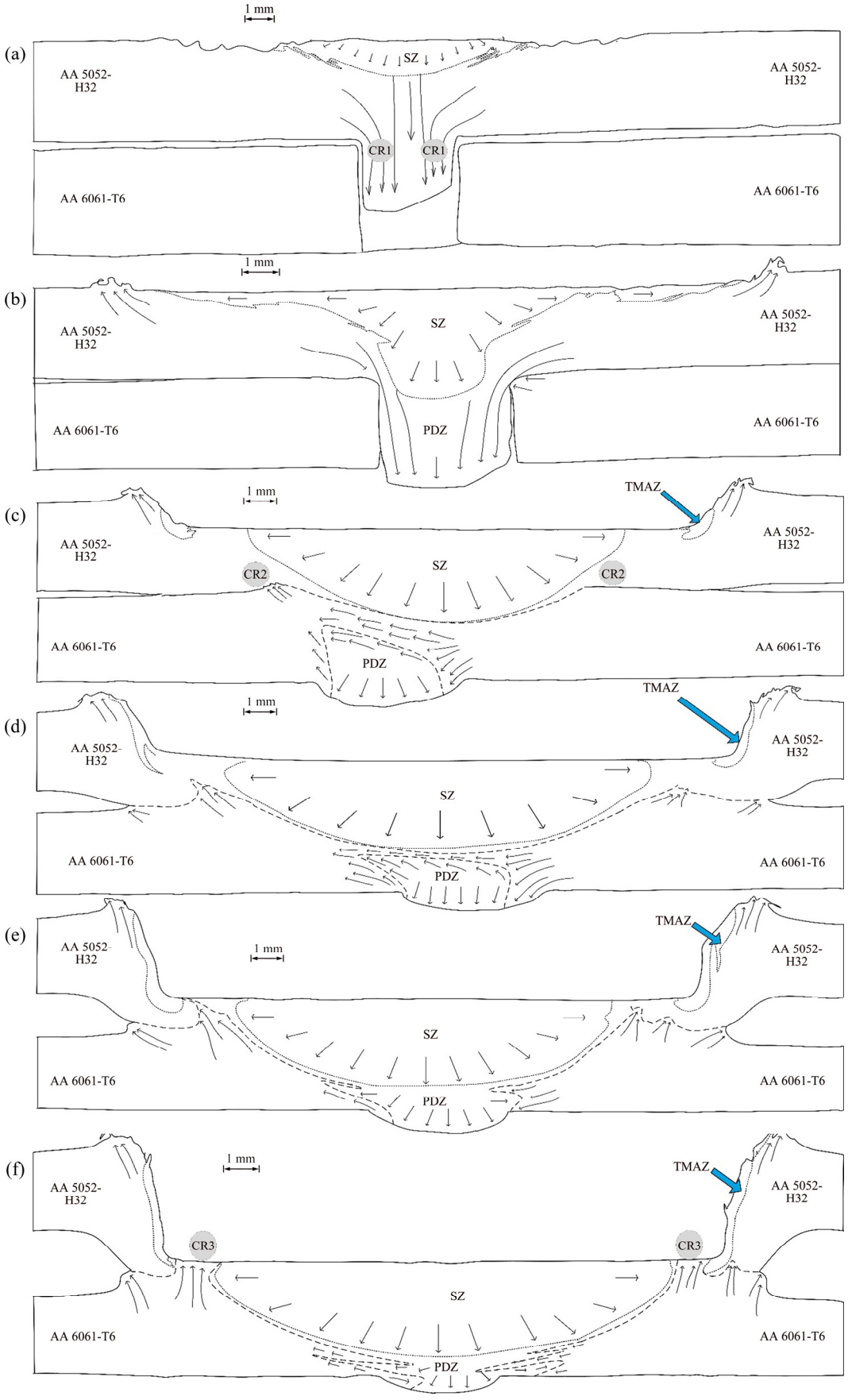

Fig. 9 Metal flow directions during FSF at different TPDs: (a) 0.2 mm; (b) 0.3 mm; (c) 0.5 mm; (d) 0.7 mm; (e) 0.9 mm; (f) 1.1 mm

mechanical interlocking are absent, indicating TPDs to be insufficient. At higher TPDs (0.9 and 1.1 mm), the formation of critical weak zones (CR3) deteriorates the performance, in spite of having metallurgical bonding and mechanical interlocking. Table 5 describes the evolution of joint formation with TPD.

An optimum TPD range of 0.5−0.7 mm is suitable to fabricate a strong joint made of AA 5052-H32 and AA 6061-T6 sheets, as suggested by the evolution of joint macrostructure. The same optimum range can be selected from mechanical performance tests like lap shear test and cross-tension test as well. There is a slight deviation in the optimum range of TPD from the peel test. In peel test, the joint strength is almost uniform in a larger range of TPD, from 0.3 to 0.7 mm, making the range flexible.

3.3 Hardness variation

Hardness variation in FSF samples can be analyzed by comparing the hardness profile over the cross-section of selected FSF samples from lower (0.2 mm), medium (0.5 mm) and higher (1.1 mm) TPDs. It is observed that the hardness of upper array and lower array of indentations has reduced from the parent metal hardness due to frictional heat flux and softening of base material.

Figure 10(a) shows the comparison of hardness along the upper array of indentation with TPD. It can be observed that FSF samples show similar hardness profile at the center of the cross-section, (locations E−K), which shows that the effect of TPD on the formation of SZ is almost similar. SZ possesses minimal hardness at the center and hardness increases towards its periphery. Since the material at the center of the SZ can freely be pushed towards the pre-drilled hole, comparatively softer regions are generated at the center than the surroundings. Moreover, the variation in hardness along the upper array with increase in the TPD is random.

Figure 10(b) shows the comparison of hardness along the lower array at different TPDs. At 0.2 mm TPD, minimum hardness for the lower array is recorded on the soft extruded pin (at Location 20, which is a part of the upper sheet). Higher hardness recorded at other locations shows that these regions are not significantly affected by the low heat flux from the SZ. At 0.5 mm TPD, the highest hardness is recorded at the closure of the pre-drilled hole (at Location T), which has compressed in between the separated pin extrudate and the upper sheet. Similar hardness profile observed at 1.1 mm TPD shows that the compression of the deformed pin by the downward movement of the tool has resulted in the

Table 5 Summary of evolution of features of FSF joint

Feature	At lower TPD	At medium TPD	At higher TPD
Pin interlock	Visible	Nil	Nil
Metallurgical bonding	Nil	Visible	Visible
SZ	Small-sized	Medium-sized	Large-sized
PDZ	Visible	Nil	Nil
TMAZ	Nil	Small-sized	Medium-sized
Pin extrudate	Partial pin formation	Disconnected pin formation	Compressed pin
Upper sheet flash	Small-sized	Medium-sized	Large-sized
Lower sheet flash	Nil	Nil	Small-sized
Upward bulging of upper sheet	Nil	Small-sized	Medium-sized
Upward distortion of lower sheet/upper sheet thinning	Nil	Visible	Severe

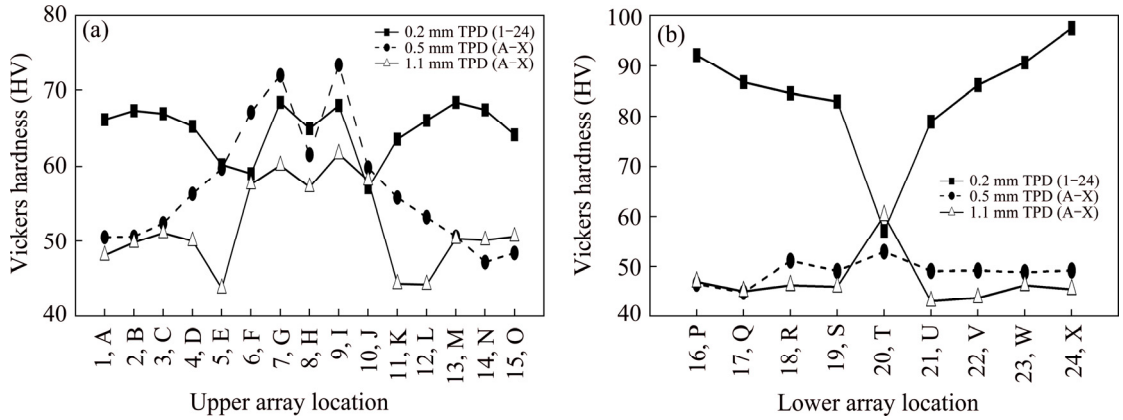

Fig. 10 Comparison of hardness variation along cross section: (a) Upper array of indentation; (b) Lower array of indentation (Typical hardness variation at each measurement location is ±1.96)

increase in the hardness at Location T. At 0.5 and 1.1 mm TPDs, hardness at all locations of the lower array, other than Location T, has reduced considerably from the parent metal hardness due to the influence of high heat flux from the SZ.

In summary, the increase in TPD has significantly affected the hardness along the lower array, while upper array possessed identical trend. Upper array shows that stir zone formation is identical at all TPDs and lower array shows that the heat flux generated from the stir zone, with increasing TPD has reduced the hardness of the lower sheet.

3.4 Joint morphology analysis

The comparison of morphological features in the FSF joint cross-section is described in this section. It is observed that the pin width and pin height, which determine the anvil cavity filling, remain almost same for FSF joints when the TPD is varied from 0.5 to 1.1 mm (Figs. 11(a) and (b)). Uniform pin width and pin height ensure that the anvil cavity filling is complete from 0.5 mm TPD onwards. At lower TPDs, the pin formation is absent, since the extrudate has not reached up to the anvil cavity. This shows that TPD has significant influence on the formation of the external pin interlock.

Upper sheet bulging is a distortion defect seen in FSF due to the constraining effect of fixture clamps that restrict the thermal expansion of upper sheet in length direction of the sample (Fig. 11(c)). The stirring and high axial plunge force result in excessive upward protrusion

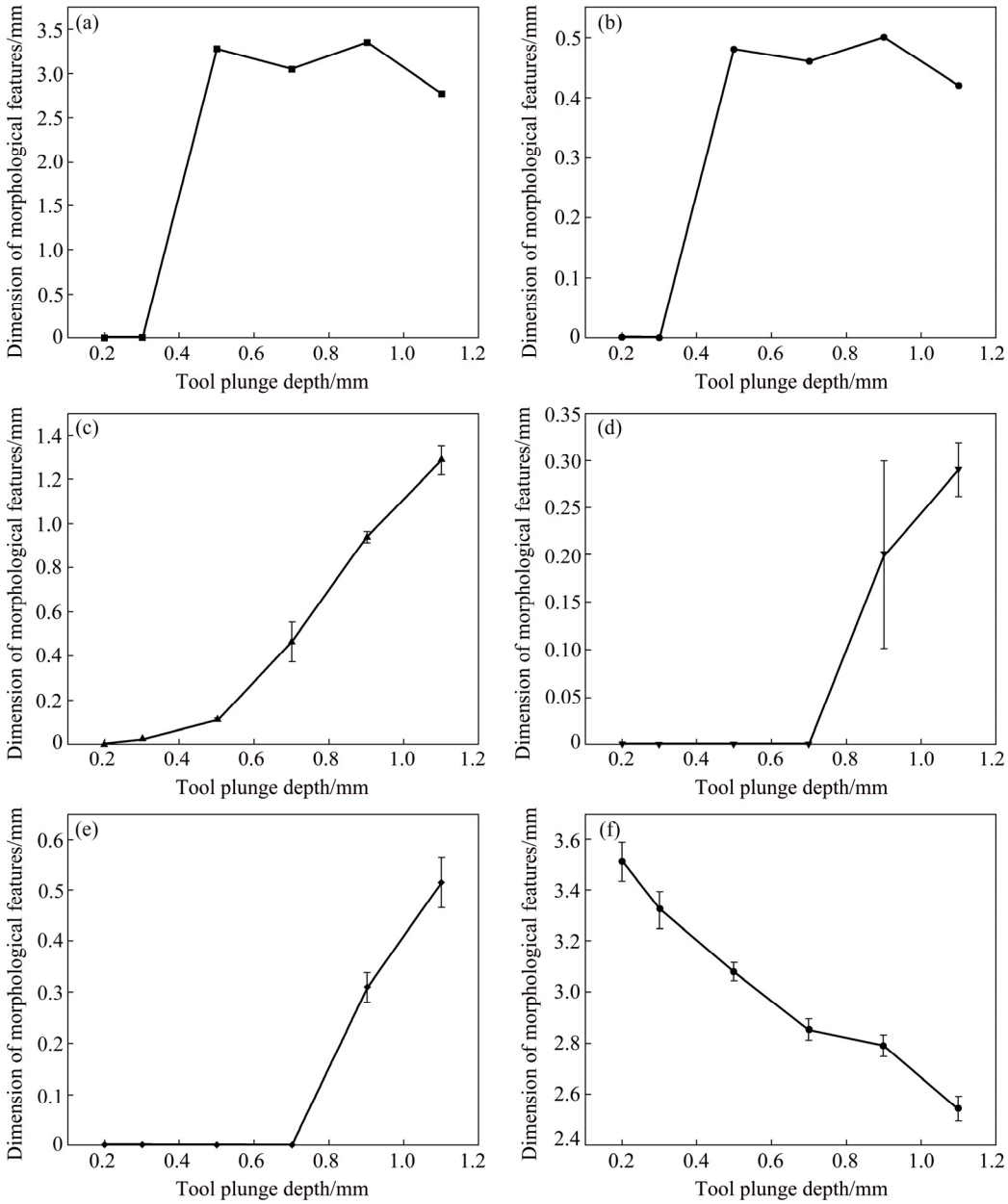

Fig. 11 Comparison of joint morphological features at various TPDs: (a) Pin width; (b) Pin height; (c) Upper sheet bulging; (d) Lower sheet flash width; (e) Lower sheet flash height; (f) Stir spot thickness

of upper sheet surrounding the lateral surface of the tool. Upper sheet bulging possesses more or less linearly increasing relationship with the TPD. It is minimal at 0.3 mm TPD, about 0.025 mm, and maximum at the highest TPD, about 1.28 mm. However, the UB values are less in this TPD range, so that its influence on the aesthetic appearance of the FSF joint is not considerable.

Flash is generally a deformation occurring in the upper and lower sheets, where the material is free to bulge out in any direction. Lower sheet flash typically forms when the lower sheet has undergone significant deformation under the heat flux from the upper sheet stir zone and the tool plunge force. It is observed that lower sheet flash has formed only at higher TPDs (0.9 and 1.1 mm), where the width and height of the flash show an increase in size with increase in the TPD (Figs. 11(d) and (e)). Therefore, it is revealed that the tool plunge depth has a direct influence on the deformation of the lower sheet and further flash formation. The upper sheet flash is not considered in this work because its formation does not directly or indirectly influence the joint formation.

From Fig. 11(f), it is revealed that stir spot thickness has an inverse relation with tool plunge depth. With increase in TPD, the material underneath the tool has moved sidewards, resulting in the decrease of stir spot thickness.

The morphological analysis shows that the variation of the joint features is significant and they are dependent on the TPD during FSF joint formation. At optimum TPDs, namely 0.5 and 0.7 mm, the morphological features such as pin width and pin height are constant, there is no flash formation and upper sheet bulging and stir spot thickness are moderate.

3.5 Modes of failure during mechanical testing

The following failure modes are observed for FSF samples in lap shear test, cross-tension test, peel test and tensile test, as shown in Fig. 12.

1) Partial bond delamination failure. The bonded region undergoes incomplete delamination, finally leaving the extruded pin and some bonded region at the stir spot over the upper sheet (Fig. 12(a)). This mode of failure is attributed to the poor metallurgical bonding in the stir spot even though proper pin formation occurs.

2) Pin shear. Pin undergoes shearing along the neck leaving the broken part inside the pre-drilled hole (Fig. 12(b)). Pin shear occurs for FSF samples, where the extruded pin interlock solely contributes the strength of the joint.

3) Combined pin shear and bond delamination. Pin undergoes severe deformation or failure along with delamination of the metallurgical bonding (Fig. 12(c)). This occurs when the pin extrudate and the metallurgical bonding share the load.

4) Tear-off. The upper sheet has undergone tearing off over the circumference of the stir spot leaving the complete bonded region stuck on the lower sheet (Fig. 12(d)). This happens mainly due to the thinning of the upper sheet during the upward distortion of the lower sheet, irrespective of proper pin formation.

5) Pin pull-out. Pin gets pulled out from the pre-drilled hole due to poor interlocking and due to the absence of metallurgical bonding (Fig. 12(e)). Pin pull-out can happen even under no load conditions. This occurs when the pin has not extruded up to the anvil cavity at lower TPDs.

6) Combined partial bond delamination and sheet tear. In addition to the bond delamination, the shearing of the lower sheet can occur from the pre-drilled hole (Fig. 12(f)). This occurs commonly when the sheets are peeled apart under tensile load.

7) Stir spot fracture. It occurs when the sample fails at the stir spot, the critical geometrical inhomogeneity in the tensile samples (Fig. 12(g)). It can be observed that the load is equally shared by both the sheets in the tensile sample.

8) Base metal fracture. It occurs when one of the sheets adjacent to the FSF joint, commonly upper sheet near the stir spot, undergoes premature failure leading to the complete failure of the tensile sample (Fig. 12(h)). Base metal fractures when the strength of the sheet adjacent to the joint in the gauge length region is less than the joint strength.

The main reason behind the failure modes in lap shear, cross-tension and peel tests are the weak zone formation at critical regions of the FSF joint. The three critical regions are 1) the neck of the pin, CR1 (Fig. 9(a)), 2) incomplete metallurgical bonding, CR2 (Fig. 9(c)) and 3) the upward distortion of the lower sheet which separates the central stir zone from the side walls of the stir spot, CR3 (Fig. 9(f)). Sometimes the neck of the pin (CR1) is so weak that shearing can happen along its neck, which leads to pin shear failure. Whenever the metallurgical bonding is incomplete (CR2) up to the stir spot circumference, the interfacial delamination initiates from the weakest region, which results in partial bond delamination failure. In some cases, the tool plunge is so severe that the upward distortion of the lower sheet (CR3) creates weaker zone near the surface of the stir spot by upper sheet thinning, which results in tear-off failure. Combined failure modes occur more or less due to the formation of more than one critical zones.

Table 6 shows the summary of the failure modes, at various TPDs, from 0.2 to 1.1 mm, of FSF samples prepared for lap shear, cross-tension, peel and tensile tests. Tear-off is the most common failure mode followed by pin pull-out. It should be noted that FSF

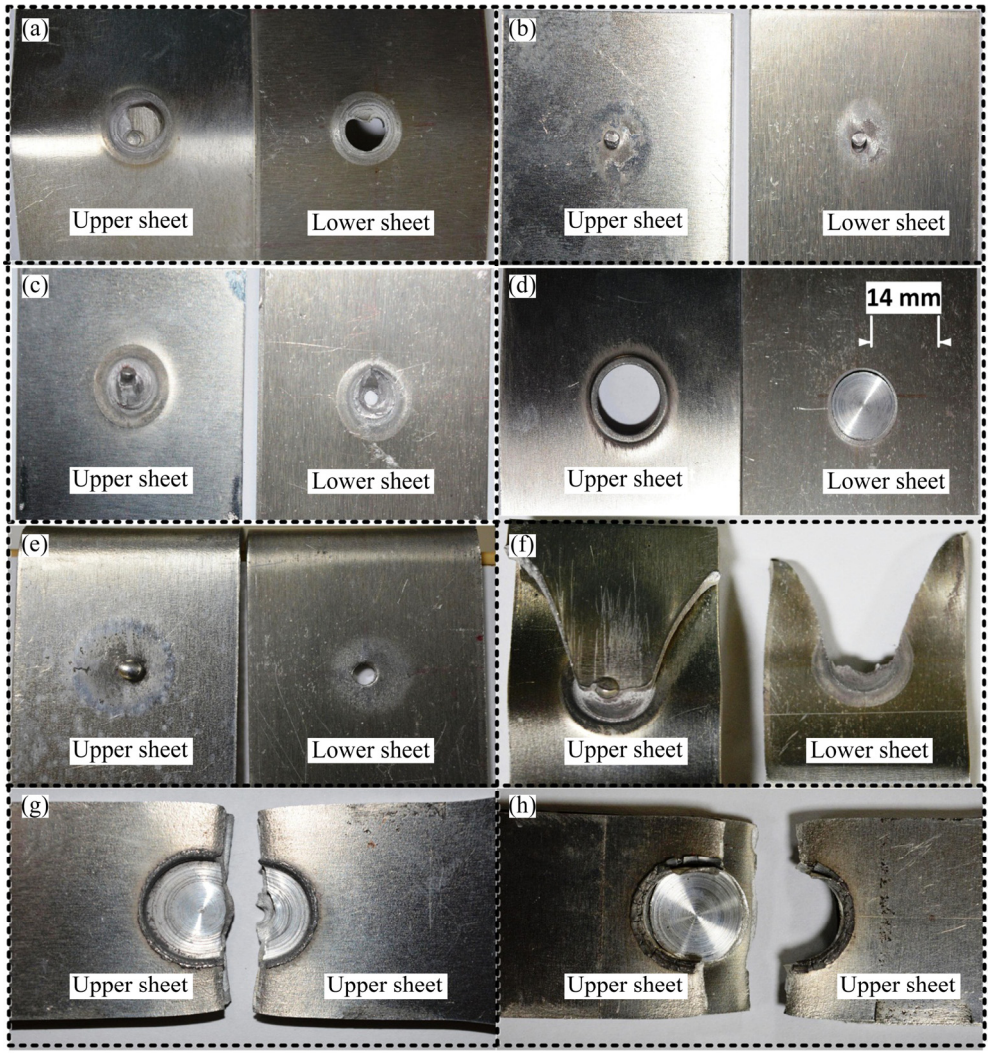

Fig. 12 Modes of failure during testing of FSF joints: (a) Partial bond delamination; (b) Pin shear; (c) Combined pin shear and bond delamination; (d) Tear-off; (e) Pin pull-out; (f) Combined partial bond delamination and sheet tear; (g) Stir spot fracture; (h) Base metal fracture

Table 6 Modes of failure

Tool plunge depth		Lap shear test		Cross-tension test		Peel test		Tensile test	
		Trial 1	Trial 2	Trial 1	Trial 2	Trial 1	Trial 2	Trial 1	Trial 2
Lower	0.2	Pin shear	Pin shear	Pin pull-out at no load	Pin pull-out at no load	Pin pull-out	Pin pull-out	Stir spot fracture	Pin pull-out at no load
	0.3	Pin shear+ Bond delamination	Pin shear	Pin pull-out	Pin pull-out	Partial bond delamination+ Sheet tear	Partial bond delamination+ Sheet tear	Base metal fracture	Base metal fracture
Medium	0.5	Tear-off	Pin shear	Partial bond delamination	Tear-off	Partial bond delamination+ Sheet tear	Tear-off	Base metal fracture	Stir spot fracture
	0.7	Tear-off	Tear-off	Tear-off	Tear-off	Tear-off	Tear-off	Base metal fracture	Stir spot fracture
Higher	0.9	Tear-off	Tear-off	Tear-off	Tear-off	Tear-off	Tear-off	Base metal fracture	Stir spot fracture
	1.1	Tear-off	Tear-off	Tear-off	Tear-off	Tear-off	Tear-off	Base metal fracture	Stir spot fracture

samples fabricated at medium and higher TPDs, from 0.7 to 1.1 mm, show tear-off failure in most cases because the major part of the strength is contributed by the metallurgical bonding. FSF samples fabricated at lower TPDs, from 0.2 to 0.5 mm, show pin pull-out failure. Therefore, the modes of failure have significant relation with the tool plunge depth. Moreover, the failure modes are random with respect to trials at same tool plunge depth for a particular test, specifically at lower and medium TPDs. The tensile test samples show entirely different modes of failure. Base metal fracture and stir spot fracture occur at random at medium and higher TPDs.

4 Conclusions

1) FSF can be successfully used to join sheet metals of almost same quality, namely AA 5052-H32 and AA 6061-T6, in which obtained lap shear strength of 7.16 kN is far better than that of other friction based joining technologies like FSW and FSSW.

2) The mechanical performance studies such as lap shear test and cross-tension test revealed that there is an optimum TPD range (0.5−0.7 mm) at which joint strength is maximum and extensibility is optimum. Peel strength of FSF samples remains almost equal throughout the range of TPDs, while formability decreases with increase in TPD during uniaxial tensile tests.

3) Macrostructure analysis revealed that metallurgical bonding and pin interlocking at different TPDs govern the joint performance during mechanical testing. Low TPDs result in poor mechanical interlocking between the upper and lower sheets. Moderate TPDs mark the beginning of metallurgical bonding, which contributes the highest joint strength and extensibility. At higher TPDs, metallurgical bonding and mechanical interlocking contribute the joint strength. Nevertheless, the inferior joint strength of FSF joints at higher TPDs is due to the formation of critical weak zone by the upward distortion of the lower sheet.

4) Hardness measurement over the cross-section of FSF samples revealed that the effect of TPD on the formation of stir zone is almost alike and the heat flux generated from the stir zone has considerably reduced the hardness of the lower sheet at medium and higher TPDs.

5) Joint morphology analysis revealed that TPD has a significant influence on the formation of external features developed on the FSF joint. Certain features such as upper sheet bulging and stir spot thickness possess linearly increasing and linearly decreasing relationships with the TPD respectively. It is also observed that lower sheet flash formation is negligible and the anvil cavity filling is complete, at optimum TPD range of 0.5−0.7 mm.

6) Failure mode analysis revealed that three critical regions, which lead to various failure modes, are the neck of the pin, incomplete metallurgical bonding and upward distortion of the lower sheet. FSF samples fabricated at medium and high TPDs show tear-off failure and those at lower TPDs show pin pull-out failure. Moreover, base metal fracture and stir spot fracture are observed randomly for FSF samples subjected to uniaxial tensile test. This shows that TPD has a significant influence on the failure modes of FSF samples.

Thus, the optimum TPD to obtain a strong joint with acceptable extension for AA 5052-H32–AA 6061-T6, of 2 mm in thicknesses, is in the moderate range from 0.5 to 0.7 mm, for which good metallurgical bonding is observed. Therefore, it can be concluded that TPD has a significant influence on the formation of FSF joint in aluminum alloys, which is clearly revealed from the mechanical performance tests, macrostructure analysis, hardness measurement, morphological studies and the failure mode analysis.

Acknowledgements

The authors thank the mechanical testing facility extended by Central Instruments Facility, IIT Guwahati for conducting the mechanical performance tests.

References

[1] RAO H M, YUAN W, BADARINARAYAN H. Effect of process parameters on mechanical properties of friction stir spot welded magnesium to aluminum alloys [J]. Materials and Design, 2015, 66: 235−245.

[2] BAEK S W, CHOI D H, LEE C Y, AHN B W, YEON Y M, SONG K, JUNG S B. Microstructure and mechanical properties of friction stir spot welded galvanized steel [J]. Materials Transactions, 2010, 51(5): 1044−1050.

[3] MITLIN D, RADMILOVIC V, PAN T, CHEN J, FENG Z, SANTELLA M L. Structure–properties relations in spot friction welded (also known as friction stir spot welded) 6111 aluminum [J]. Materials Science and Engineering A, 2006, 441: 79−96.

[4] TUTAR M, AYDIN H, YUCE C, YAVUZ N, BAYRAM A. The optimization of process parameters for friction stir spot-welded AA3003-H12 aluminum alloy using a Taguchi orthogonal array [J]. Materials and Design, 2014, 63: 789−797.

[5] BOZZI S, HELBERT-ETTER A L, BAUDIN T, KLOSEK V, KERBIGUET J G, CRIQUI B. Influence of FSSW parameters on fracture mechanisms of 5182 aluminum weld [J]. Journal of Materials Processing Technology, 2010, 210: 1429−1435.

[6] YOON S O, KANG M S, KWON Y J, HONG S T, PARK D H, LEE K H, LIM C Y, SEO J D. Influences of tool plunge speed and tool plunge depth on friction spot joining of AA5454-O aluminum alloy plates with different thicknesses [J]. Transactions of Nonferrous Metals Society of China, 2012, 22: 629−633.

[7] PICCINI J M, SVOBODA H G. Effect of the tool penetration depth in friction stir spot welding (FSSW) of dissimilar aluminum alloys [J]. Procedia Materials Science, 2015, 8: 868−877.

[8] PATHAK N, BANDYOPADHYAY K, SARANGI M, PANDA S K. Microstructure and mechanical performance of friction stir spot-welded aluminum-5754 sheets [J]. Journal of Materials Engineering and Performance, 2013, 22(1): 131−144.
[9] YUSOF F, MIYASHITA Y, SEO N, MUTOH Y, MOSHWAN R. Utilizing friction spot joining for dissimilar joint between aluminum alloy (A5052) and polyethylene terephthalate [J]. Science and Technology of Welding and Joining, 2012, 17(7): 544−549.
[10] ARICI A, MERT S. Friction stir spot welding of polypropylene [J]. Journal of Reinforced Plastics and Composites, 2004, 27(18): 2001−2004.
[11] NISHHARA T. Development of friction stir forming [J]. Material Science Forum, 2003, 426−432: 2971−2978.
[12] NISHIHARA T, ITO A. Measurement of die temperature during friction stir forming [J]. Welding in the World, 2005, 49(3−4): 22−26.
[13] BALAKRISHNAN K N, KANG H T, MALLICK P K. Joining aluminum to nylon using frictional heat [R]. SAE Technical Paper, 2007, 2007-01-1701.
[14] LAZAREVIC S, MILLER SF, LI J, CARLSON BE. Experimental analysis of friction stir forming for dissimilar material joining application [J]. Journal of Manufacturing Processes, 2013, 15: 616−624.
[15] LAZAREVIC S, OGATA K A, MILLER S F, KRUGER G H, CARLSON B E. Formation and structure of work material in the friction stir forming process [J]. Journal of Manufacturing Science and Engineering, 2015, 137/051018: 1−9.
[16] AHUJA Y, IBRAHIM R, PARADOWSKA A, RILEY D. Friction stir forming to fabricate copper–tungsten composite [J]. Journal of Materials Processing Technology, 2015, 217: 222−231.
[17] OGATA K A, LAZAREVIC S, MILLER S F. Dissimilar material joint strength and structure for friction stir forming process [C]// ProcASME 2014. Detroit, MI: MSEC, 2014: 9−13.
[18] DAS H, CHAKRABORTY D, KUMAR PAL T. High-cycle fatigue behavior of friction stir butt welded 6061 aluminum alloy [J]. Transactions of Nonferrous Metals Society of China, 2014, 24: 648−656.
[19] ILANGOVAN M, BOOPATHY S R, BALASUBRAMANIAN V. Microstructure and tensile properties of friction stir welded dissimilar AA6061−AA5086 aluminum alloy joints [J]. Transactions of Nonferrous Metals Society of China, 2015, 25: 1080−1090.
[20] HEJAZI I, MIRSALEHI S E. Mechanical and metallurgical characterization of AA6061 friction stir welded joints using microhardness map [J]. Transactions of Nonferrous Metals Society of China, 2016, 26: 2313−2319.
[21] HEJAZI I, MIRSALEHI S E. Effect of pin penetration depth on double-sided friction stir welded joints of AA6061-T913 alloy [J]. Transactions of Nonferrous Metals Society of China, 2016, 26: 676−683.
[22] SAJU T P, NARAYANAN R G. Effect of tool rotational speed on the mechanical performance of joints fabricated by friction stir forming of dissimilar grade aluminum alloys [C]//Proc AIMTDR 2016. Pune, India: AIMTDR, 2016: 921−925.
[23] KUMBHAR N T, BHANUMURTHY K. Friction stir welding of Al 5052 with Al 6061 alloys [J]. Journal of Metallurgy, 2012, 303756.
[24] RAJKUMAR V, VENKATESHKANNAN M, SADEESH P, ARIVAZHAGAN N, RAMKUMAR K D. Studies on effect of tool design and welding parameters on the friction stir welding of dissimilar aluminum alloys AA 5052−AA 6061 [J]. Procedia Engineering, 2014, 75: 93−97.
[25] PARK S K, HONG S T, PARK J H, PARK K Y, KWON Y J, SON H J. Effect of material locations on properties of friction stir welding joints of dissimilar aluminum alloys [J]. Science and Technology of Welding and Joining, 2010, 15(4): 331−336.
[26] JEON C S, HONG S T, KWON Y J, CHO H H, HAN H N. Material properties of friction stir spot welded joints of dissimilar aluminum alloys [J]. Transactions of Nonferrous Metals Society of China, 2012, 22: 605−613.

搅拌针压入深度对搅拌摩擦成形 AA 5052-H32 和 AA 6061-T6 金属板的接头形成和力学性能的影响

Tinu P. SAJU, R. Ganesh NARAYANAN

Department of Mechanical Engineering, Indian Institute of Technology Guwahati, Assam, 781039, India

摘　要：研究不同等级的 AA 5052-H32 和 AA 6061-T6 铝合金搅拌摩擦成形连接的可能性。结果表明，当搅拌针压入深度为 0.5~0.7 mm 时，采用万能试验机测试得到的搭接剪切载荷为 7.16 kN，横向拉伸载荷为 3.51 kN， 优于采用搅拌摩擦焊和搅拌摩擦点焊在相同材料上焊接的接头的性能。采用光学显微镜观察接头微观组织，发现接头的增强是由于机械销连锁或冶金结合。采用维氏硬度仪测量显微硬度，揭示搅拌针压入深度对搅拌区形成的作用和摩擦热流密度对低层金属薄片的影响。电子显微镜形貌显示，搅拌针压入深度对接头中机械销的形成和几何特征存在显著影响。不同的失效模式，例如销拔出、销剪切、部分结合分层和剥落，取决于不同的搅拌针压入深度形成的关键薄弱区。

关键词：搅拌摩擦成形；搅拌针压入深度；铝合金；搭接剪切试验；横向拉伸试验；失效模式

(Edited by Bing YANG)